

Eye-vergence visual servoing enhancing Lyapunov-stable trackability

Fujia Yu · Mamoru Minami · Wei Song · Akira Yanou

Received: 13 March 2012 / Accepted: 19 March 2013 / Published online: 11 May 2013
© ISAROB 2013

Abstract Visual servoing methods for hand–eye configuration are vulnerable for hand’s dynamical oscillation, since nonlinear dynamical effects of whole manipulator stand against the stable tracking ability (trackability). Our proposal to solve this problem is that the controller for visual servoing of the hand and the one for eye-vergence should be separated independently based on decoupling each other, where the trackability is verified by Lyapunov analysis. Then the effectiveness of the decoupled hand and eye-vergence visual servoing method is evaluated through simulations incorporated with actual dynamics of 7-DoF robot with additional 3-DoF for eye-vergence mechanism by amplitude and phase frequency analysis.

Keywords Visual servoing · Eye-vergence · Trackability

1 Introduction

Recently, much research attention has turned to focus on full DoF pose control of the robot end effector toward a

target object [1]. Full 3D visual servoing requires simultaneously full 3D pose measurement and 3D motion control also. But researches so far seem to have tended to deal with these two problems separately as isolated issues. Different kinds of visual servoing—position-based [2], image-based [3] or $2\frac{1}{2}$ -D visual servoing [4]—usually discuss their methodologies based on an assumption that pose measurement is known or could be easily received from some other devices.

Eye-vergence function bears two fundamental fruits as kinematical merit and dynamical one. First, kinematical merit is described. Observing ability of a fixed-hand–eye configuration may be deteriorated by relative geometry of the camera and the target, as the robot cannot observe the object well when it is near the cameras (Fig. 1a), small intersection of the possible sight space of the two cameras (Fig. 1b), and the image of the object cannot appear in the center of both cameras, so we could not get clear image information of target reflected at its periphery, reducing the pose measurement accuracy (Fig. 1c). To solve these problems, eye-vergence functions to rotate eye cameras orientation to see target object at center of the cameras’ view, as shown in Fig. 2(a–c), enhancing the measurement accuracy in trigonometric calculation and avoiding aberration, i.e., peripheral distortion of camera lens. Moreover, recent researches on visual servoing are limited generally in a swath of tracking an object while keeping a certain constant distance [3, 5, 6], which are the researches based on different task scenarios from the approaching visual servoing discussed here. The second merit is concerning dynamical effects to keep tracking a moving target in the camera’s view. Needless to say in visual servoing application, keeping closed loop of visual feedback is vital from a view point of stability in control

This work was presented in part at the 17th International Symposium on Artificial Life and Robotics, Oita, Japan, January 19–21, 2012.

F. Yu · M. Minami (✉) · A. Yanou
Graduate School of Natural Science and Technology,
Okayama University, 3-1-1 Tsushimanaka, Okayama, Japan
e-mail: minami@suri.sys.okayama-u.ac.jp

W. Song
School of Mechatronics Engineering and Automation,
Shanghai University, 149 Yanchang Road, Zhabei District,
Shanghai, China

Fig. 1 Disadvantage of fixed-camera system

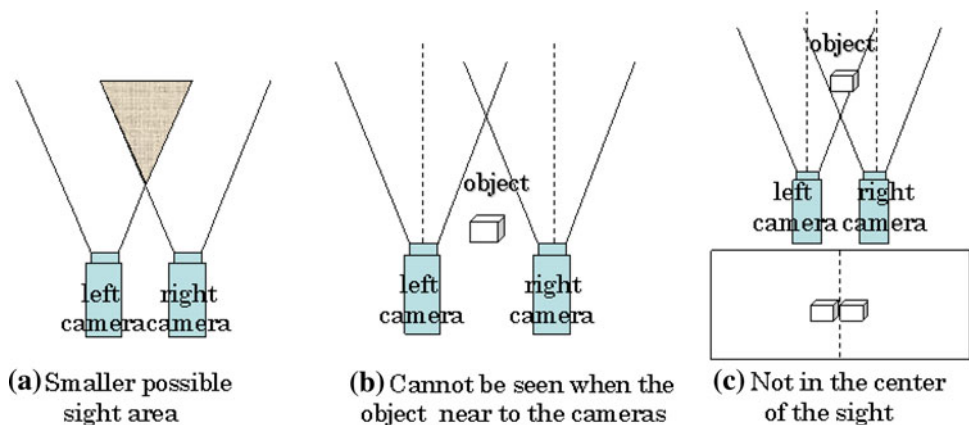
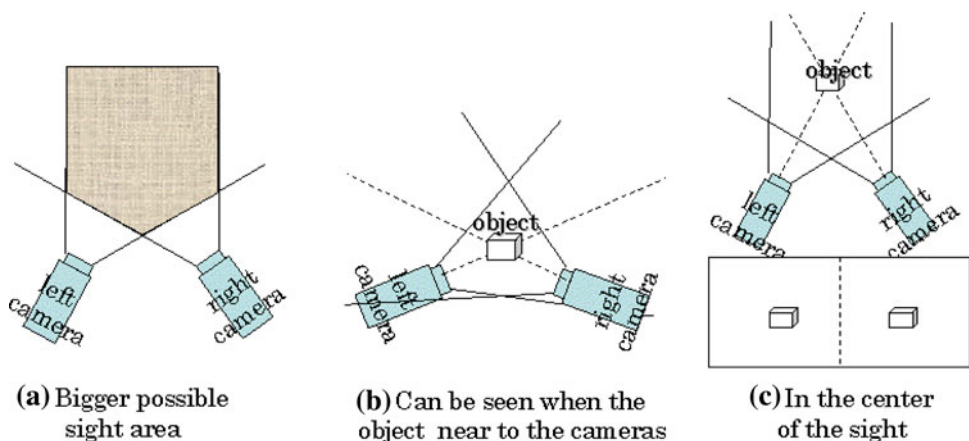


Fig. 2 Advantage of eye-vergence system



theory. Cameras fixed at the hand of manipulator are kept staring at the object at first, but when the target moves so fast that the manipulator cannot catch up with the speed of the target because of whole manipulator’s dynamics, resulting in the visual feedback cut, losing feedback. To improve this pose tracking difficulty of fixed-hand-eye system, the eye-vergence function seems dynamically effective, because of small mass and inertia moment of the eye ball compared to those of full manipulator’s structure. Therefore, tracking ability of eye-vergence can be better than fixed, like animals tracking target with eye motion before rotating their heads to the target. In this report, we propose a new control method of hand and eye-vergence dual visual servoing system with a stability analysis of Lyapunov method, guaranteeing that both the tracking pose errors of hand and eye-vergence orientation error converge to zero, providing target object stopping in work space. Further to evaluate the trackability through frequency response experiment, we need a new measure to rate the eye’s trackability to the target object oscillating with designated amplitude and angular velocity. We also come up with a yardstick to measure the eye’s trackability.

2 Simulator and robot dynamics

The dynamics equation of the system is

$$M(q)\ddot{q} + h(q, \dot{q}) + g(q) = \tau \tag{1}$$

here q is a vector expressing the angle of each joint, where q can be divided into $q = [q_E^T, q_C^T]^T$ where q_E and q_C express the joint angles of the manipulator and the camera system, respectively, $\tau = [\tau_1^T, \dots, \tau_n^T]^T$ is the input torque, and $M(q)$ is the inertia matrix, $h(q, \dot{q})$ is the vector representing the centrifugal and coriolis forces, $g(q)$ is the vector representing the gravity load.

The simulator is based on the actual physical parameters of MITSUBISHI PA-10 robot arm. Two cameras, which have 3 degrees of freedom, are mounted on the end-effector of PA-10 robot arm. The structure of the system is shown in Fig. 3. The homogeneous transformation from coordinate static to the end effector \sum_8 to the end effector coordinate \sum_E is expressed by a constant matrix 8T_E . In this paper we use T to express homogeneous transformation matrix. \sum_9 and \sum_{10} express the coordinate of the right and left camera separately, they will be written as \sum_R

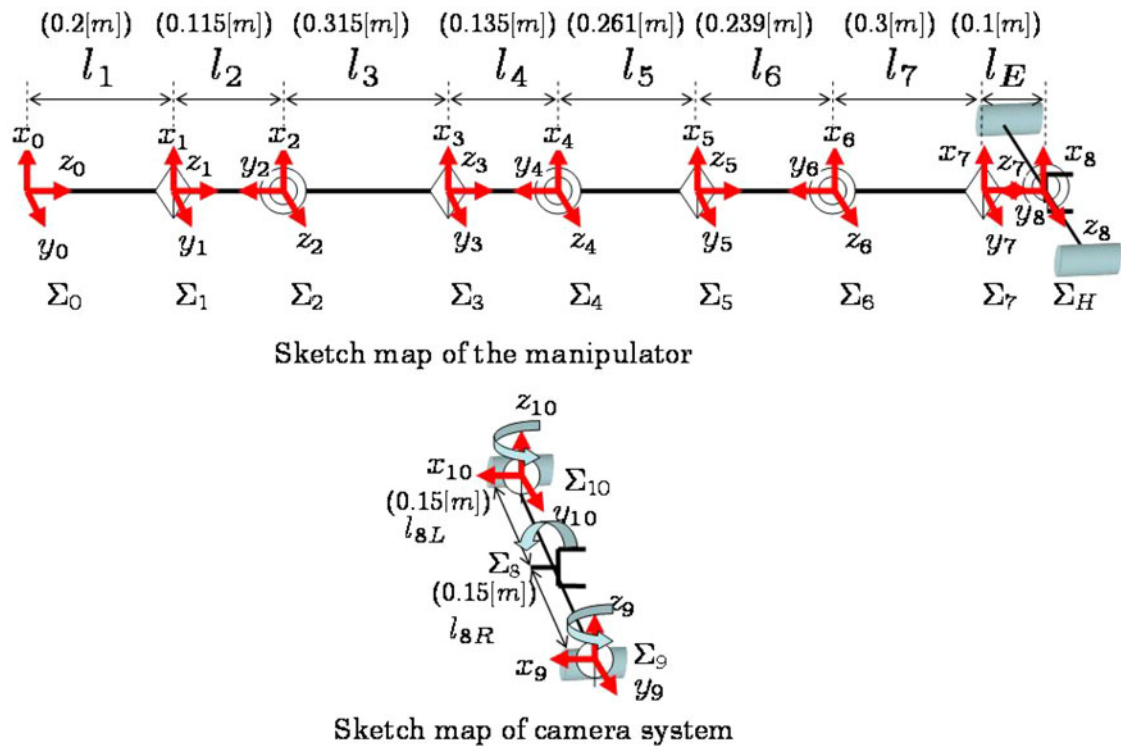


Fig. 3 Frame structure of manipulator and eye-vergence system

and Σ_L . While the two cameras are both installed on the end effector, both the cameras share a same tilt angle, but each of them has an own pan angle, angular velocity ω_i , angular acceleration $\dot{\omega}_i$, link acceleration \ddot{p}_i and the acceleration of the center of gravity \ddot{s}_i can be calculated by the method written in [7].

3 Hand and eye visual servoing

3.1 Desired trajectory

As shown in Fig. 4, the world coordinate frame is denoted by Σ_W , the target coordinate frame is denoted by Σ_M , and the desired and actual end effector coordinate frame is denoted by Σ_{Ed} and Σ_E respectively. The desired relative relation between the target and the end effector is given by homogeneous transformation as ${}^{Ed}T_M$, the relation between the target and the actual end effector is given by ${}^E T_M$, then the difference between the desired end effector pose Σ_{Ed} and the actual end effector pose Σ_E is denoted as ${}^E T_{Ed}$, and calculated by:

$${}^E T_{Ed}(t) = {}^E T_M(t) {}^{Ed} T_M^{-1}(t) \tag{2}$$

Equation (2) is a general deduction that satisfies arbitrary object motion ${}^W T_M(t)$ and arbitrary visual servoing objective ${}^{Ed} T_M(t)$. However, the relation ${}^E T_M(t)$

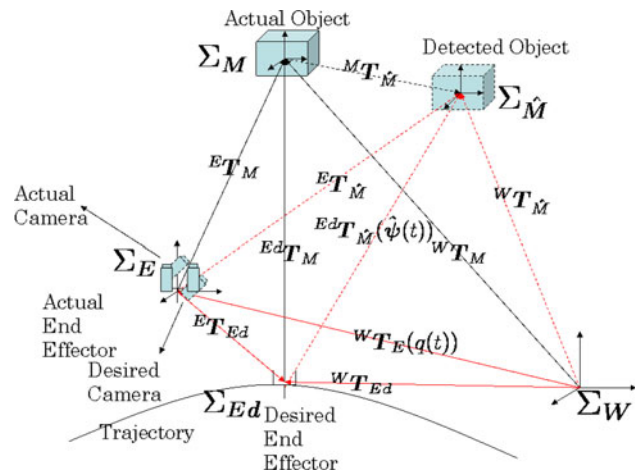


Fig. 4 Motion of the end effector and object

is only observed by cameras using the on-line model-based recognition method and 1-step GA [8, 9]. Let $\Sigma_{\hat{M}}$ denote the detected object, there always exist an error between the actual object Σ_M and the detected one $\Sigma_{\hat{M}}$. However, in visual servoing we use different methods to decrease this error. For example, we can limit the error inside 5[mm] in [10]. So in visual servoing, Eq. (2) will be rewritten based on $\Sigma_{\hat{M}}$ that includes the error ${}^M T_{\hat{M}}$, as

$${}^E T_{Ed}(t) = {}^E T_{\hat{M}}(t) {}^{Ed} T_M^{-1}(t) \tag{3}$$

where ${}^E T_{\hat{M}}(t) = {}^E T_M(t)$ which is determined by the given visual servoing objective. Differentiating Eq. (3) with respect to time twice,

$${}^E \ddot{T}_{Ed}(t) = {}^E \ddot{T}_M(t) {}^M T_{Ed}(t) + 2 {}^E \dot{T}_M(t) {}^M \dot{T}_{Ed}(t) + {}^E T_{\hat{M}}(t) {}^M \ddot{T}_{Ed}(t) \quad (4)$$

where ${}^M T_{Ed}$, ${}^M \dot{T}_{Ed}$, ${}^M \ddot{T}_{Ed}$ are given as the desired visual servoing objective. ${}^E T_{\hat{M}}$, ${}^E \dot{T}_{\hat{M}}$, ${}^E \ddot{T}_{\hat{M}}$ can be observed by cameras. From these preparations, we can calculate the variables in the controllers of the system in the next subsection, such as Δp_E and so on, leaving detailed explanation for the next subsection. As shown in Fig. 4, there are two errors that we should decrease to the value as small as possible in the visual servoing process. First one is the error between the actual object and the detected one ${}^M T_{\hat{M}}$, and the other is the error between the desired end effector and the actual one, ${}^E T_{Ed}$. In our research, the error of ${}^M T_{\hat{M}}$ is decreased by on-line recognition method of 1-step GA, MFF compensation method and the eye-vergence camera system, and the error of ${}^E T_{Ed}$ can be decreased by the hand visual servoing controller.

3.2 Hand desired acceleration

The block diagram of our proposed hand and eye-vergence visual servoing controller is shown in Fig. 5. The hand visual servoing is the outer loop. The controller used for hand visual servoing is proposed by Siciliano and Villani [11]. First we will introduce the variables defined in the system:

$$\Delta p_E = p_d - p_E \quad (5)$$

here d and E in the bottom right corner of the p mean the desired position and actual position of the end effector. There is no letter in the top left corner, it

means the vector or the matrix is expressed in the world frame.

A special type of angle/axis representation of the orientation error is obtained with the quaternion, i.e.

$${}^E \eta = \cos \frac{\theta_{Ed}}{2} \quad (6)$$

$${}^E \Delta \varepsilon = \sin \frac{\theta_{Ed}}{2} {}^E k_{Ed} \quad (7)$$

here θ and k are the rotation angle and the rotation axis of the object. The letter in the top left corner expresses the coordinate where the vector or the rotation matrix is expressed in, while the angle velocity error between the desired and the actual angle velocity is defined as:

$$\Delta \omega_E = \omega_d - \omega_E \quad (8)$$

With the variables defined above, we just show main equations of the hand visual servoing controller that are used to calculate input torque τ .

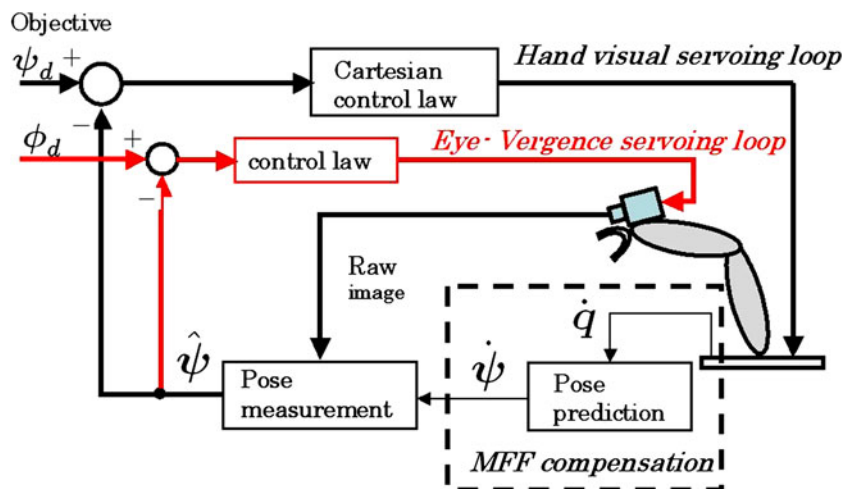
$$a_{pE} = \ddot{p}_d + K_{Dp} \Delta \dot{p}_E + K_{Pp} \Delta p_E \quad (9)$$

$$a_{oE} = \dot{\omega}_d + K_{Do} \Delta \omega_E + K_{Po} R_E {}^E \Delta \varepsilon \quad (10)$$

$$s_E = J_E^+(q_E) \{ a_E - J_E(q_E, \dot{q}_E) \dot{q}_E \} + \{ I - J_E^+(q_E) J_E(q_E) \} \{ E_p(q_{Ed} - q_E) + E_d(\dot{q}_{Ed} - \dot{q}_E) \} \quad (11)$$

here, \ddot{p}_d is a 3×1 vector representing the desired acceleration of the end effector of the PA-10 manipulator. a_E is the end effector desired velocity which can express the position and orientation, respectively, as $[a_{pE}^T, a_{oE}^T]^T$. The quaternion error from the actual orientation to the desired orientation of the end effector ${}^E \Delta \varepsilon$ can be extracted from the transformation ${}^E T_{Ed}$, and the other error variables in Eqs. (9, 10) are described in \sum_W , which can be calculated by the transformation ${}^E T_{Ed}$, ${}^E \dot{T}_{Ed}$, ${}^E \ddot{T}_{Ed}$ in Eqs. (3, 4),

Fig. 5 Hand and eye visual servoing system



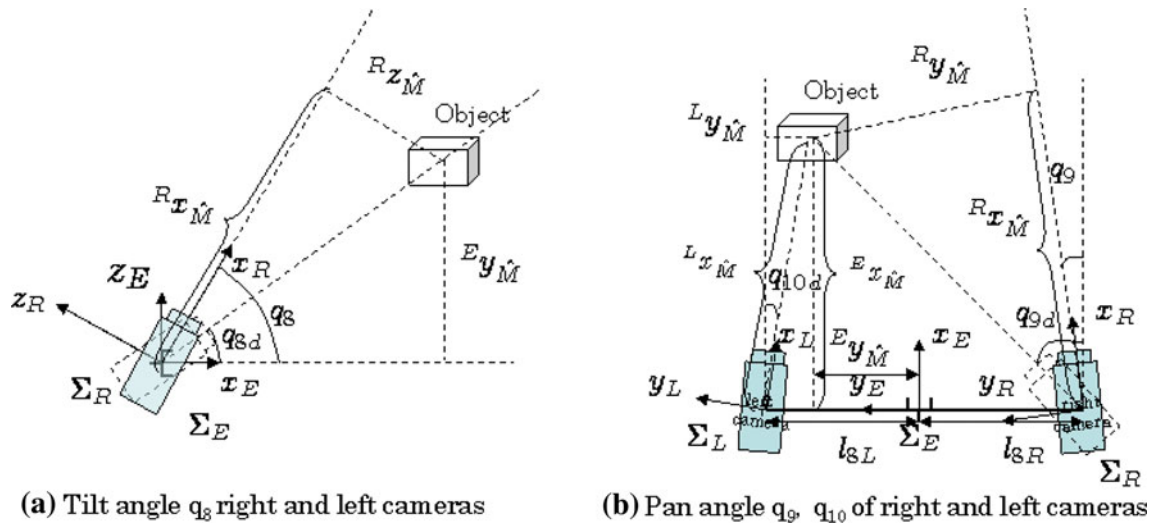


Fig. 6 Pan and tilt camera angles defined based on relation between target object and cameras

using the rotational matrix R_E through coordinate transformation.

And $J_E(q_E)$ is the Jacobian matrix from the world coordinate to the end effector, which means that $\omega_E = J_E(q_E)q_E$, and $J_E^+(q_E)$ in Eq. (11) is the pseudo-inverse of $J_E(q_E)$ given by $J_E^+(q_E) = J_E^T(J_E J_E^T)^{-1}$. K_{D_p} , K_{P_p} , K_{D_o} , K_{P_o} are positive control gains.

3.3 Eye-vergence desired acceleration

The eye-vergence visual servoing is the inner loop of the visual servoing system shown in Fig. 5. In this paper, we use two pan-tilt cameras for eye-vergence visual servoing. Here, the positions of cameras are supposed to be fixed on the end effector. For camera system, q_8 is tilt angle, q_9 and q_{10} are pan angles, and q_8 is common for both cameras. As it is shown in Fig. 6, ${}^E x_M, {}^E y_M, {}^E z_M$ express position of the detected object in the end effector coordinate. The desired angle of the camera joints $q_{Cd} = [q_{8d}, q_{9d}, q_{10d}]^T$ can be calculated by:

$$q_{8d} = a \tan 2({}^E y_M, {}^E z_M) \tag{12}$$

$$q_{9d} = a \tan 2(-l_{8R} + {}^E x_M, {}^E z_M) \tag{13}$$

$$q_{10d} = a \tan 2(l_{8L} + {}^E x_M, {}^E z_M) \tag{14}$$

where $l_{8L} = l_{8R} = 150[\text{mm}]$ is the camera location, we set the center line of a camera as the z axis of each camera coordinate, so the object will be in the center of the sight of the right camera when ${}^R x_M = 0$ and ${}^R y_M = 0$. Here ${}^R x_M, {}^R y_M, {}^R z_M$ express the position of the detected object in the right camera coordinate.

$$\Delta q_C = q_{Cd} - q_C \tag{15}$$

$$s_C = \ddot{q}_{Cd} + K_{D_c} \Delta \dot{q}_C + K_{P_c} \Delta q_C \tag{16}$$

here K_{D_c}, K_{P_c} are positive definite diagonal matrices.

3.4 Hand/eye-vergence controller

By the desired accelerations from Eqs. 11, 16), input τ is calculated by:

$$s = \begin{bmatrix} s_E \\ s_C \end{bmatrix} \tag{17}$$

$$\tau = M(q)s + h(q, \dot{q}) + g(q) \tag{18}$$

here if we submit the input torque into the dynamics equation Eq. (1) we can get the output acceleration equal to the desired one which will be discussed in detail later.

4 Stability of hand and eye-vergence motion

4.1 Manipulator dynamics

We discuss about the convergence of our proposed hand visual servoing system. From the input torque of each joint in Eq. (18) and the dynamics equation of the system Eq. (1)

$$\ddot{q} = s \tag{19}$$

so

$$\ddot{q}_E = s_E \tag{20}$$

Take Eq. (11) (here we do not consider the second item in the right side which is the controller of the redundancy) into Eq. (20) we have

$$a_E = J_E(q_E)\ddot{q}_E + \dot{J}_E(q_E, \dot{q}_E)\dot{q}_E \tag{21}$$

so

$$\begin{bmatrix} \ddot{p}_E \\ \ddot{\omega}_E \end{bmatrix} = J_E(q_E)\ddot{q}_E + \dot{J}_E(q_E, \dot{q}_E)\dot{q}_E \tag{22}$$

which means

$$\begin{bmatrix} \ddot{\mathbf{p}}_E \\ \dot{\boldsymbol{\omega}}_E \end{bmatrix} = \begin{bmatrix} \mathbf{a}_{pE} \\ \mathbf{a}_{\omega E} \end{bmatrix}. \tag{23}$$

Submit \mathbf{a}_{pE} , $\mathbf{a}_{\omega E}$ in Eq. (23) into Eqs. (9, 10),

$$\Delta\ddot{\mathbf{p}}_E + \mathbf{K}_{D_p}\Delta\dot{\mathbf{p}}_E + \mathbf{K}_{P_p}\Delta\mathbf{p}_E = \mathbf{0} \tag{24}$$

$$\Delta\dot{\boldsymbol{\omega}}_E + \mathbf{K}_{D_\omega}\Delta\boldsymbol{\omega}_E + \mathbf{K}_{P_\omega}\mathbf{R}_E^E\Delta\boldsymbol{\varepsilon} = \mathbf{0} \tag{25}$$

4.2 Camera dynamics

For the cameras, from Eq. (19),

$$\ddot{\mathbf{q}}_C = \mathbf{s}_C \tag{26}$$

from Eq. (16), the close loop becomes:

$$\Delta\ddot{\mathbf{q}}_C + \mathbf{K}_{D_C}\Delta\dot{\mathbf{q}}_C + \mathbf{K}_{P_C}\Delta\mathbf{q}_C = \mathbf{0} \tag{27}$$

4.3 Stability analysis

We invoke a Lyapunov argument, the feed back gains are taken as scalar matrices, i.e. $\mathbf{K}_{D_p} = \mathbf{K}_{D_p}I$, $\mathbf{K}_{P_p} = \mathbf{K}_{P_p}I$, $\mathbf{K}_{D_\omega} = \mathbf{K}_{D_\omega}I$ and $\mathbf{K}_{P_\omega} = \mathbf{K}_{P_\omega}I$. Here we assume that the feedback gains of the links are the same.

$$\begin{aligned} V = & \Delta\mathbf{p}_E^T\mathbf{K}_{P_p}\Delta\mathbf{p}_E + (\Delta\dot{\mathbf{p}}_E)^T\Delta\dot{\mathbf{p}}_E + \mathbf{K}_{P_\omega}\{(\eta - 1)^2 \\ & + (\Delta\boldsymbol{\varepsilon})^T\Delta\boldsymbol{\varepsilon}\} + \frac{1}{2}(\Delta\boldsymbol{\omega}_E)^T\Delta\boldsymbol{\omega}_E + \Delta\mathbf{q}_C^T\mathbf{K}_{P_C}\Delta\mathbf{q}_C \\ & + (\Delta\dot{\mathbf{q}}_C)^T\Delta\dot{\mathbf{q}}_C \geq 0 \end{aligned} \tag{28}$$

so

$$\begin{aligned} \dot{V} = & 2\Delta\dot{\mathbf{p}}_E^T(\Delta\ddot{\mathbf{p}}_E + \mathbf{K}_{P_p}\Delta\dot{\mathbf{p}}_E) + 2\mathbf{K}_{P_\omega}\{(\eta - 1)\dot{\eta} + (\Delta\boldsymbol{\varepsilon})^T\Delta\dot{\boldsymbol{\varepsilon}}\} \\ & + (\Delta\dot{\boldsymbol{\omega}}_E)^T\Delta\dot{\boldsymbol{\omega}}_E + 2\Delta\dot{\mathbf{q}}_C^T(\Delta\ddot{\mathbf{q}}_C + \mathbf{K}_{P_C}\Delta\dot{\mathbf{q}}_C) \end{aligned} \tag{29}$$

From Eq. (24) we can know that

$$\Delta\ddot{\mathbf{p}}_E + \mathbf{K}_{P_p}\Delta\dot{\mathbf{p}}_E = -\mathbf{K}_{D_p}\Delta\dot{\mathbf{p}}_E. \tag{30}$$

from the quaternion definition we can know that

$$\dot{\eta} = -\frac{1}{2}(\Delta\boldsymbol{\varepsilon})^T\Delta\boldsymbol{\omega}_E \tag{31}$$

and

$$\Delta\dot{\boldsymbol{\varepsilon}} = \frac{1}{2}\mathbf{E}(\eta, \Delta\boldsymbol{\varepsilon})\Delta\boldsymbol{\omega}_E \tag{32}$$

where $\mathbf{E}(\eta, \boldsymbol{\varepsilon}) = \eta\mathbf{I} - \mathbf{S}(\boldsymbol{\varepsilon})$. $\mathbf{S}(\mathbf{a})$ is a anti-symmetric matrix that satisfies $\mathbf{S}(\mathbf{a})\mathbf{b} = \mathbf{a} \times \mathbf{b}$.

From Eq. (27) we can get:

$$\Delta\ddot{\mathbf{q}}_C + \mathbf{K}_{P_C}\Delta\dot{\mathbf{q}}_C = -\mathbf{K}_{D_C}\Delta\dot{\mathbf{q}}_C \tag{33}$$

Substitute Eqs. (25), (30–33) into Eq. (29) we can get:

$$\dot{V} = -2\Delta\dot{\mathbf{p}}_E^T\mathbf{K}_{D_p}\Delta\dot{\mathbf{p}}_E - \Delta\boldsymbol{\omega}_E^T\mathbf{K}_{D_\omega}\Delta\boldsymbol{\omega}_E - 2\Delta\dot{\mathbf{q}}_C^T\mathbf{K}_{D_C}\Delta\dot{\mathbf{q}}_C \leq 0 \tag{34}$$

here, because \mathbf{K}_{D_p} , \mathbf{K}_{D_ω} and \mathbf{K}_{D_C} are positive definite, only if $\Delta\dot{\mathbf{p}}_E = \mathbf{0}$, $\Delta\boldsymbol{\omega}_E = \mathbf{0}$ and $\Delta\dot{\mathbf{q}}_C = \mathbf{0}$, $\dot{V} = \mathbf{0}$, so $\Delta\ddot{\mathbf{p}}_E = \mathbf{0}$, from Eq. (24), $\Delta\dot{\mathbf{p}}_E = \mathbf{0}$. For the same reason, when $\Delta\dot{\mathbf{q}}_C = \mathbf{0}$, $\Delta\ddot{\mathbf{q}}_C = \mathbf{0}$ from Eq. (27), $\Delta\dot{\mathbf{q}}_C = \mathbf{0}$. When $\Delta\boldsymbol{\omega}_E = \mathbf{0}$, $\Delta\dot{\boldsymbol{\omega}}_E = \mathbf{0}$. And from Eq. (25) ${}^E\Delta\boldsymbol{\varepsilon} = \mathbf{0}$. The definition domain of θ is $(-\pi, \pi)$, so the manipulator and the cameras asymptotically converge to the invariant sets s .

$$s = \{ \Delta\mathbf{p}_E = \mathbf{0}, \Delta\dot{\mathbf{p}}_E = \mathbf{0}, \eta = 1, {}^E\Delta\boldsymbol{\varepsilon} = \mathbf{0}, \Delta\boldsymbol{\omega}_E = \mathbf{0}, \Delta\mathbf{q}_C = \mathbf{0}, \Delta\dot{\mathbf{q}}_C = \mathbf{0} \} \tag{35}$$

so

$$\lim_{t \rightarrow \infty} {}^E\mathbf{T}_{Ed} = \mathbf{I} \lim_{t \rightarrow \infty} {}^E\dot{\mathbf{T}}_{Ed} = \mathbf{0} \tag{36}$$

substitute Eqs. (36 to 3),

$$\lim_{t \rightarrow \infty} {}^E\mathbf{T}_{M} = \lim_{t \rightarrow \infty} {}^{Ed}\mathbf{T}_{M} \tag{37}$$

and from Eqs. (12 to 14)

$$\lim_{t \rightarrow \infty} {}^Rz_{M} = 0, \lim_{t \rightarrow \infty} {}^Ry_{M} = 0, \lim_{t \rightarrow \infty} {}^Ly_{M} = 0 \tag{38}$$

which means the object will come to the center line of the cameras, which means that the object will always come to the center of the sight of the cameras.

5 Simulation of hand and eye-vergence visual servoing

To verify the effectiveness of the proposed hand and eye visual servoing system, we conduct the experiment of visual servoing to a 3D marker that is composed of a red

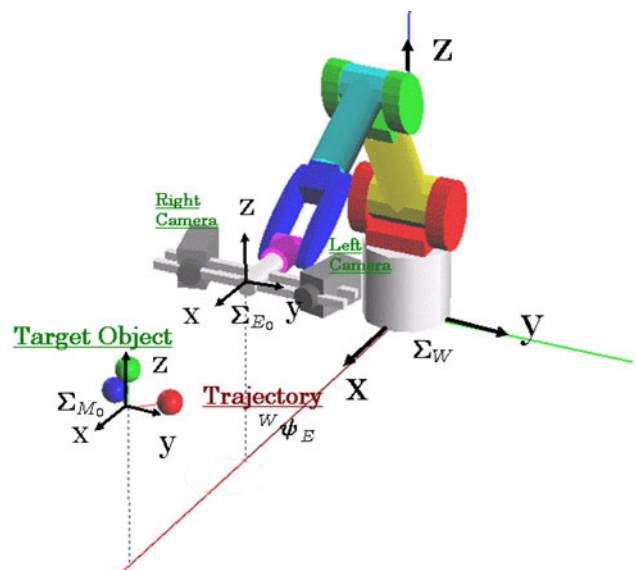


Fig. 7 Object and the visual servoing system

ball, a green ball and a blue ball as Fig. 7. The radiuses of these three balls are set as 30[mm].

5.1 Simulation condition

The recognition error does not affect the dynamic error, so we assume that ${}^M T_{\hat{M}} = I$. The position and orientation of the target object are given to the robot directly in the simulation. The initial hand pose is defined as Σ_{E_0} , while the initial object pose is defined as Σ_{M_0} , and the homogeneous.

Transform matrix from Σ_W to Σ_{M_0} is:

$${}^w T_{M_0} = \begin{bmatrix} 0 & 0 & -1 & -1410[\text{mm}] \\ 1 & 0 & 0 & 0[\text{mm}] \\ 0 & -1 & 0 & 355[\text{mm}] \\ 0 & 0 & 0 & 1 \end{bmatrix} \quad (39)$$

The target object moves according to the following time function

$${}^{M_0} \psi_M = [0, 200 \sin(\omega t)[\text{mm}], 0, 0, 0, 0]^T \quad (40)$$

here, ω is the angular velocity of the motion of the object.

The relation between the object and the desired end effector is set as:

$${}^{M_0} \psi_M = [500[\text{mm}], 0, 0, 0, 0, 0]^T \quad (41)$$

The controller gain of the system K_{D_p} , K_{P_p} , K_{D_o} , K_{P_o} are affected by the mass, initial moment, the amplifier output and many other conditions. From the common sense because the camera mass is smaller than the manipulator, K_{D_c} and K_{P_c} can be set bigger than K_{D_p} , etc. Here $K_{P_c} = \text{diag}\{5, 5, 5\}$, $K_{D_c} = \text{diag}\{3, 3, 3\}$, and $K_{D_p} = K_{P_p} = K_{D_o} = K_{P_o} = \text{diag}\{1, 1, 1\}$.

5.2 Definition of trackability

5.2.1 Camera trackability

Here, to compare the trackability of the eye-vergence system and fixed-camera system, we define a concept of gazing point. As it is shown in Fig. 8 the intersection of the gazing line of right camera and the $y_{M_0} - z_{M_0}$ plane is defined as the gazing point. The relative relation between Σ_{M_0} and Σ_R is given by homogeneous transformation as ${}^{M_0} T_R$, ${}^{M_0} T_R$ concludes the rotation matrix ${}^{M_0} R_R$ and the position vector ${}^{M_0} p_R$, and the rotation matrix ${}^{M_0} R_R$ can be written as $[{}^{M_0} x_R, {}^{M_0} y_R, {}^{M_0} z_R]$. The direction of ${}^{M_0} l_R$ in Fig. 8 is same as the direction of x_R , and ${}^{M_0} l_R$ can be expressed as:

$${}^{M_0} l_R = {}^{M_0} p_R + k_R {}^{M_0} x_R \quad (42)$$

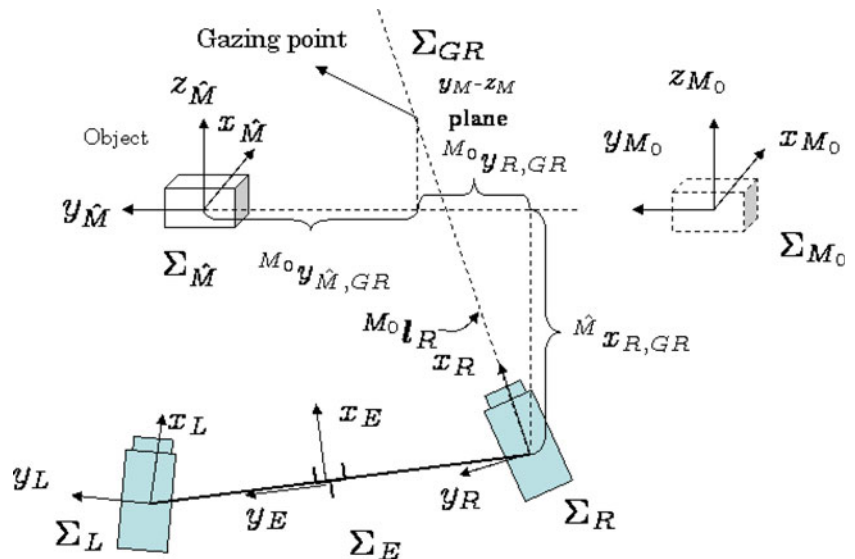
here k_R is a scalar variable. The gazing point of the right camera expressed in Σ_{M_0} is ${}^{M_0} p_R = [0, {}^{M_0} y_R, {}^{M_0} z_R]^T$. For ${}^{M_0} l_R = {}^{M_0} p_R$ in x direction, $({}^{M_0} p_R)_x + k_R ({}^{M_0} x_R)_x = 0$. And usually $({}^{M_0} x_R)_x \neq 0$, k_R can be calculated by $k_R = -({}^{M_0} p_R)_x / ({}^{M_0} x_R)_x$, and they, z coordinate of the gazing point in Σ_{M_0} can be calculated by:

$${}^{M_0} y_{GR} = ({}^{M_0} p_R)_y + k_R ({}^{M_0} x_R)_y \quad (43)$$

$${}^{M_0} z_{GR} = ({}^{M_0} p_R)_z + k_R ({}^{M_0} x_R)_z \quad (44)$$

The target object's motion is given by Eq. (40), because the motion of the target object M is parallel to the y_{M_0} , we take ${}^{M_0} y_M(t)$ as the input, and the gazing point of the right camera ${}^{M_0} y_{GR}(t)$ as the response. And define the concept of trackability by the frequency response of ${}^{M_0} y_{GR}(t)$, the trackability of the left camera can be defined in the same way.

Fig. 8 Camera's and end effector's gazing point



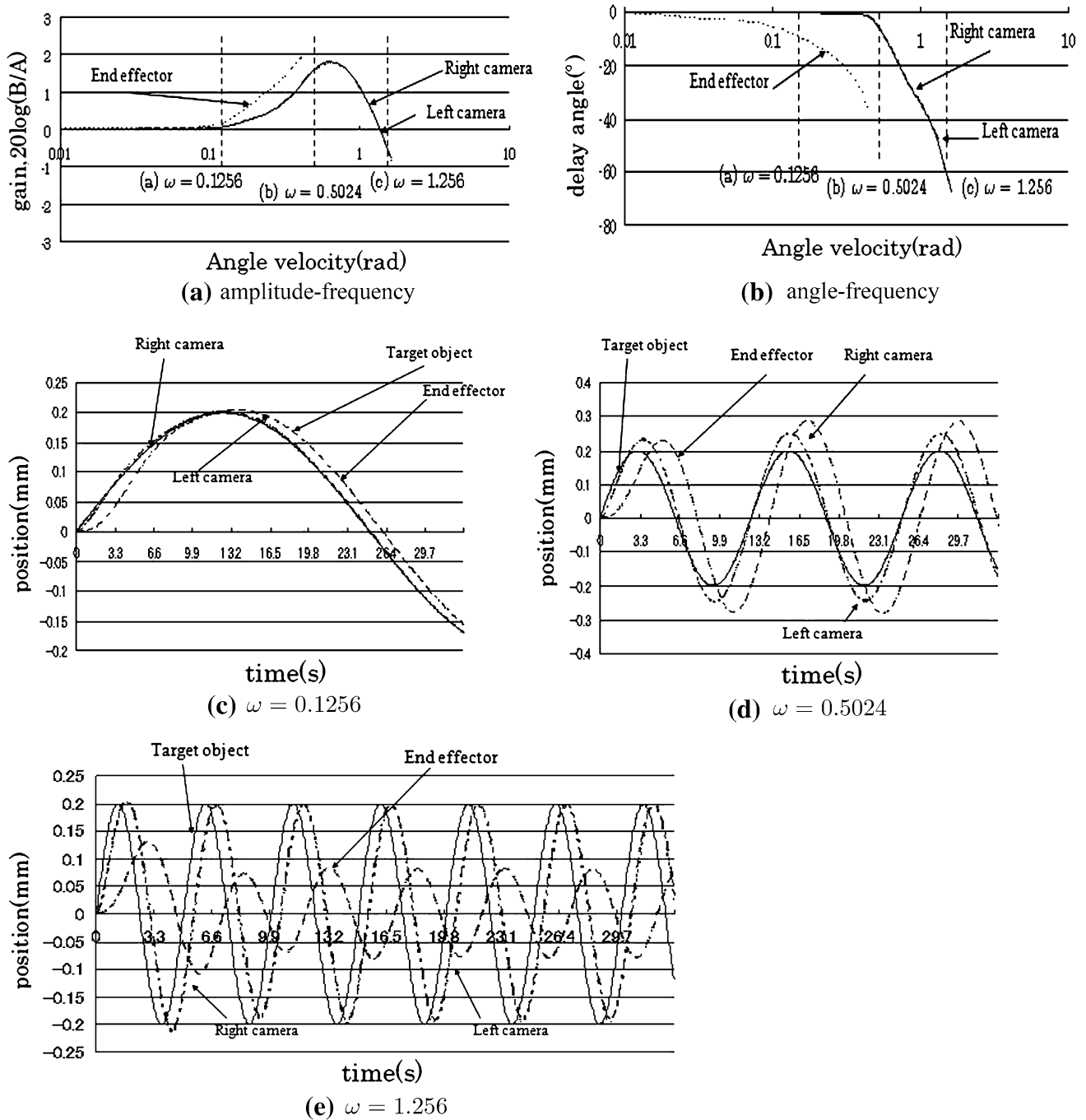


Fig. 9 Comparison of camera's and end effector's trackabilities by frequency response

5.2.2 End effector trackability

To compare with the trackability of the camera, it is necessary to define the End effector trackability. Here the gazing line direction of normal static hand-eye system is same as the x direction of \sum_E , so the gazing point of the static hand-eye system is same as the gazing point of the end effector, the similar evaluation method is also used in [12].

5.3 Simulation results

The original position of the target object ${}^W T_{M_0}$ is given by Eq. (39), the target object motion function is Eq. (40). The desired relation between the end effector and the target object is given in Eq. (41). The ω in Eq. (40) changes from 0.01 to 2.00. In Fig. 9, we show the result of our experiment. The amplitude-frequency curve and the delay

frequency curve are shown in Fig. 9(a, b). Here, for the fixed camera $A = \max(M_0 y_M(t))$, $B = \max(M_0 y_{GE}(t))$. For the right camera of eye-vergence system $A = \max(M_0 y_M(t))$, $B = \max(M_0 y_{GR}(t))$, for the left camera $A = \max(M_0 y_M(t))$, $B = \max(M_0 y_{GL}(t))$. In these two figures the abscissa axes are logarithmic scalar of ω . In Fig. 9(a, b), we sign the angular velocity when $\omega = 0.1256, 0.5024, 1.256$, and show the position of the gazing point of the cameras in eye-vergence simulation and the position of the gazing point of the end effector in fixed-camera experiment in Fig. 9(c–e). We can see that both the fixed-camera system and eye-vergence system can track the target object when $\omega = 0.1256$ while the fixed-camera system cannot track the target object when $\omega > 0.5024$ so in e, and the eye-vergence system can track the target object even when $\omega = 1.256$.

From Fig. 9a we can see the data of the cameras and the end effector all become bigger as ω increases for the reason of resonance, but the curve of the fixed-camera system is always below the curves of the cameras, we can see that the amplitude of the eye-vergence system is more closed to the target object than the fixed-camera system, the fixed-camera system cannot track the target object when $\omega > 0.5024$, so the point line disappear near $\omega = 0.5024$, while in eye-vergence system the fastest velocity of the target object under which the system can catch up with is 1.6956. From Fig. 9b the curve of the fixed-camera system is also below the curves of the cameras, which means that delay of the fixed-camera system is bigger than the eye-vergence system, To be understood easily, we show the position of the gazing point of the cameras in eye-vergence experiment and the position of the gazing point of the end effector in fixed-camera experiment in Fig. 9(c–e). From the figures it is also easy to see that comparing with the fixed-camera system, the eye-vergence system can track the target object better.

6 Conclusion

In this paper, we propose a concept of trackability to evaluate the observation ability on a moving object of

visual servoing system. We get amplitude–frequency and phase–frequency curves of the cameras of the eye-vergence system and the fixed-camera system under moving object with different angular velocity in simulation and get the conclusion that the trackability and stability of the eye-vergence system are better than those of the fixed-camera system.

References

1. Hutchinson S, Hager G, Corke P (1996) A tutorial on visual servo control. *IEEE Trans Robotics Autom* 12(5):651–670
2. Sepp W, Fuchs S, Hirzinger G (2006) Hierarchical featureless tracking for position-based 6-DoF visual servoing. In: *Proceedings of the 2006 IEEE/RSJ International Conference on Intelligent Robotics and Systems (IROS)*, pp 4310–4315
3. Tahri O, Chaumette F (2005) Point-based and region-based image moments for visual servoing of planar objects. *IEEE Trans Robotics* 21(6):1116–1127
4. Malis E, Chaumette F, Boudet S (1999) 2-1/2-D visual servoing. *IEEE Trans Robotics Autom* 15(2):238–250
5. Song W, Minami M, Mae Y, Aoyagi S (2007) On-line evolutionary head pose measurement by feedforward stereo model matching. In: *Proceedings of IEEE International Conference Robotics Automation (ICRA)*, pp 4394–4400
6. Hamel T, Mahony R (2002) Visual servoing of an under-actuated dynamic rigid-body system: an Image-based approach. *IEEE Trans Robotics Autom* 18(2):187–198
7. Yoshikawa T “Foundations of Robotics: analysis and control”, ISBN 0-262-24028-9
8. Song W, Yu F, Minami M (2010) 3D visual servoing by feedforward evolutionary recognition. *J Adv Mech Des Syst Manuf (JAMDSM)* 4(4):739–755
9. Song W, Minami M, Aoyagi S (2007) On-line stable evolutionary recognition based on unit quaternion representation by motion-feedforward compensation. *Int J Intell Comput Med Sci Image Process (IC-MED)* 2(2):127–139
10. Minami M, Song W (2009) Hand-eye-motion invariant pose estimation with on-line 1-step GA -3D pose tracking accuracy evaluation in dynamic hand–eye oscillation. *J Robotics Mechatron* 21(6):709–719
11. Siciliano B, Villani L (2000) *Robot Force Control*, ISBN 0-7923-7733-8
12. Yu F, Song W, Minami M, Yanou A (2011) Frequency response of 3-D full-tracking visual servoing experiment with eye-vergence. In: *Proceedings of IECON*, pp 106–111